Coherent-incoherent transition and relaxation in condensed-phase tunneling systems

C. H. Mak* and David Chandler
Department of Chemistry, University of California, Berkeley, California 94720
(Received 15 April 1991)

The tunneling dynamics of the spin-boson problem has been computed using discretized path-integral simulations for temperatures T and couplings, i.e., the Kondo parameter α, spanning the entire T-α plane. The inherent problem of alternating weights has been solved using a combination of the stationary-phase Monte Carlo method and contour-distortion techniques. A transition from coherent to purely incoherent relaxation was observed for the spin correlation function. The time correlation functions and the location of the coherent-incoherent boundary on the T-α plane are well described by the noninteracting-blip approximation. In the deep-tunneling limit of large α, low T, and high bath frequency, the system relaxes exponentially, with its relaxation time constant following a power-law temperature dependence, in accord with perturbation theory. At higher T and low bath frequency, the relaxation time crosses over to a classical Arrhenius temperature dependence, reflecting the onset of activated processes. For a narrow region within $\frac{1}{2}<\alpha<1$, numerical results suggest that the system undergoes incoherent relaxation, with a short-time exponential decay, followed by a long-time tail of the power-law type. The short-time exponential relaxation time follows a peculiar power-law temperature dependence, with the relaxation rate increasing as a function of decreasing temperature.

I. INTRODUCTION

Studies of tunneling systems in condensed phases are important for many areas of physics and chemistry. For example, the rate of oxidation-reduction reactions at low temperatures are dominated by electron tunneling between donor and acceptor sites [1]. Tunneling of protons, on the other hand, is responsible for the transport of hydrogen trapped in crystal lattices [2]. Quantum tunneling can also be observed macroscopically, such as in Josephson junctions at low temperatures [3] and in rf superconducting quantum interference devices [4].

In the studies of quantum tunneling in double-well systems at low temperatures, it is sufficient to restrict our attention to the lowest two eigenstates of the unperturbed tunneling system. Within this truncated state space, the tunneling system is described by the two-level system Hamiltonian

$$H_0=-K\sigma_x \ , \tag{1.1}$$

where σ_i $(i=x,y,z)$ are the Pauli matrices, $2K$ is the tunnel splitting, and the basis is chosen so that the eigenstate of σ_z with eigenvalue $+1$ corresponds to the system being localized in the left well and eigenvalue -1 in the right well. The two-level system described by Eq. (1.1) is highly nonlinear and its dynamics evolves purely through quantum tunneling. In isolation, the two-level system exhibits perfect quantum coherence at all temperatures, which is reflected by the sinusoidal oscillations in the spin correlation function $C(t)=\mathrm{Re}\langle\sigma_z(0)\sigma_z(t)\rangle$.

The effects of dissipation can be introduced by coupling the two-level system to an infinite set of harmonic oscillators through σ_z to describe solvation. The Hamiltonian of the coupled system is

$$H=H_0+H_B+\phi\sigma_z \ , \tag{1.2}$$

where

$$H_B=\sum_j\left[\frac{p_j^2}{2m_j}+\frac{m_j\omega_j^2x_j^2}{2}\right] , \tag{1.3}$$

and m_j and ω_j are the mass and frequency of the jth oscillator. The local field

$$\phi=\sum_j c_jx_j \ , \tag{1.4}$$

where c_j is the strength of the coupling to the jth oscillator. Complete knowledge of the effects of the environment is captured in the "spectral density"

$$J(\omega)\equiv\frac{\pi}{2}\sum_j(c_j^2/m_j\omega_j)\delta(\omega-\omega_j) \ . \tag{1.5}$$

The predominant effect of dissipation is manifested as a loss of quantum coherence in the two-level system. Equation (1.2) with Eqs. (1.3) and (1.4) is often called the spin-boson Hamiltonian [5–14].

A class of models that have been studied extensively in the past assumes a power-law form for the spectral density,

$$J(\omega)=\eta\omega^s\exp(-\omega/\omega_c) \ . \tag{1.6}$$

The so-called "Ohmic" dissipation with $s=1$ exhibits a great variety of behaviors and has been studied most. This model is not limited to systems coupled to bosonic baths. Even coupling to fermionic environments formed by conduction electrons at low temperatures can be described using an Ohmic dissipation [15–18]. This particular form for $J(\omega)$ ensures a well-defined classical friction

η. A dimensionless variable $\alpha \equiv 2\eta/\pi$ is often used to quantify the strength of the system-environment coupling. For a bosonic bath, α can take on any value greater than zero; for a fermionic bath, α can never exceed unity [17]. The quantity $\alpha = 2\eta/\pi$ is the Kondo parameter, often referred to as K. We, however, reserve $2K$ for the tunnel splitting; cf. Eq. (1.1).

The effects of dissipation on tunneling has been the subject of intense study in the past. Early theories were based on the "golden rule," which gives the tunneling rate in terms of an expansion in the number of kinks [8,19,20]. In the limit of a nearly adiabatic bath at high temperature, a Landau-Zener treatment can be applied giving the correction to the crossing rate due to surface hopping [1]. At low temperatures, approximate theories for both the weak-coupling limit [6,11,20,21] and the strong-coupling limit [8,11] have been formulated. In addition, a variational theory based on the adiabatic reference has been studied [13]. There have also been semiclassical approximations using bounce and instanton methods [6,20]. In various limits, these theories provide exact or nearly exact results.

Most recently, a functional integral approach using the noninteracting-blip approximation has been used to study the spin-boson model as a function of temperature T and coupling α [5]. The noninteracting-blip approximation gives exact results in a number of physically quite distinct limits, and appears to bridge gaps left by many of the previous theories. The approximation has been used in an attempt to map out the general behaviors of the spin-boson model on the T-α plane. At low temperature and small coupling, the system exhibits quantum coherence with a small incoherent background. As the coupling is increased, a transition from coherent to incoherent behavior is observed. At large coupling and/or high temperature, the system relaxes exponentially. The greatest uncertainty in these predictions exists in a region on the T-α plane for intermediate coupling and low temperature, where the relaxation is assumed to be incoherent.

Recently, we presented a Brief Report on a method to compute real-time correlation functions for the spin-boson model in the high-coupling regime using dynamical Monte Carlo path-integral methods [22]. In the present paper, we describe an extension of our earlier work to treat the spin-boson model throughout the *entire* range of coupling strengths. The goal of our current work is to test predictions of previous analytical theories against dynamical Monte Carlo path-integral simulations. By Monte Carlo, we have computed the spin correlation function for a wide region on the T-α plane. By comparing with the noninteracting-blip approximation, we show that many of the qualitative predictions of that theory are correct. We do, however, find differences, some of an apparently qualitative nature. Perhaps our numerical results will foster further analytical work.

From another point of view, we believe the present work is important for technical reasons. Previous direct path-integral simulations of real time dynamics has suffered from the "sign problem" [22–27]. The presence of complex-valued actions leads to nonpositive definite "weights" that cannot be treated by conventional Monte Carlo methods. Our goal on this technical front is to examine possible ways to deal with the sign problem. The method presented here may provide a general approach to solving this problem that may be of rather broad applicability. For the spin-boson problem itself, our approach is significant as this is the first definitive numerical treatment of the model.

In Sec. II, we describe the discretized path integrals for the spin-boson model and show that they are isomorphic to a one-dimensional Ising model with both nearest-neighbor and long-range interactions that are in general complex valued. In Sec. III, we review the general approach to simulating real-time dynamics using the stationary-phase Monte Carlo (SPMC) method [23–25]. In Sec. IV, we specialize the SPMC method to the spin-boson problem and introduce the Hubbard-Stratonovich transformation. In Sec. IV, we motivate the necessity of generalizing the SPMC method by distorting path-integration contours. Technical details related to this discussion are given in Appendix A. In Sec. VI, we briefly describe our Monte Carlo algorithm, once again deferring the details to Appendix B. In Sec. VII, the numerical results will be presented with a detailed comparison with the results of the noninteracting-blip approximation. Finally, in Sec. VIII, we summarize our observations and offer some thoughts about the future of dynamical path-integral Monte Carlo methods.

II. DISCRETIZED PATH-INTEGRAL FORMALISM

In the spin-boson model, the relevant dynamical quantity to study is the spin correlation function

$$\langle \sigma_z(0)\sigma_z(t)\rangle = Z^{-1}\,\mathrm{Tr}\, e^{-\beta H}\sigma_z e^{itH/\hbar}\sigma_z e^{-itH/\hbar}\,, \tag{2.1}$$

where $\beta = 1/k_B T$ and $Z = \mathrm{Tr}\, e^{-\beta H}$. Another correlation function $\langle h_A(0)h_A(t)\rangle$ of the projection operator $h_A = \frac{1}{2}(1+\sigma_z)$ is related to the spin correlation function by

$$\langle \sigma_z(0)\sigma_z(t)\rangle = 4\langle h_A(0)h_A(t)\rangle - 1 \tag{2.2}$$

and has the same information content as the spin correlation function. For our application, the formulation for $\langle h_A(0)h_A(t)\rangle$ proves more convenient. But the results can easily be translated back to $\langle \sigma_z(0)\sigma_z(t)\rangle$ using Eq. (2.2). The real part of $\langle \sigma_z(0)\sigma_z(t)\rangle$ is subsequently referred to as $C(t)$.

Correlation functions such as $\langle h_A(0)h_A(t)\rangle$ may be represented using discretized path integrals [14,28]

$$\langle h_A(0)h_A(t)\rangle = \frac{\mathrm{Tr}\, e^{-\beta H} h_A e^{itH/\hbar} h_A e^{-itH/\hbar}}{\mathrm{Tr}\, e^{-\beta H} e^{itH/\hbar} e^{-itH/\hbar}} \tag{2.3a}$$

$$= \frac{\int dr_1 \cdots dr_{P+2Q} \exp(\Omega[r_1,\ldots,r_{P+2Q}])\, h_A(r) h_A(r')}{\int dr_1 \cdots dr_{P+2Q} \exp(\Omega[r_1,\ldots,r_{P+2Q}])} \tag{2.3b}$$

in the coordinate representative $|r\rangle \equiv |\sigma, x_i\rangle$, where σ is the position of the two-level system, and Ω, the complex-valued action that governs the dynamics in real time, is given by a sum of three piecewise actions

$$\begin{aligned}\Omega[r_1,\ldots,r_{P+2Q}] = & S[r_1,\ldots,r_{P+1};\beta\hbar] \\ & + S[r_{P+1},\ldots,r_{P+Q+1};-i\tau] \\ & + S[r_{P+Q+1},\ldots,r_1;i\tau] \end{aligned} \tag{2.4}$$

for any real time $\tau \geq t$, and $S[r_1,\ldots,r_{N+1};\gamma\hbar]$ denotes the N-point discretized action for the imaginary-time path integral from time 0 to $\gamma\hbar$. Notice that P points have been used to parametrize the thermal path, and Q points for both the forward and reverse time paths. The indices in Eq. (2.4) are understood to be cyclic, i.e., $r_{P+2Q+1}=r_1$. It is important to note that Eq. (2.3b) is valid for *any* pair of points r and r' separated by a total time of *it* along the cycle. Also note that in writing Eq. (2.3b), we assume that P and Q are large enough that the discretized path well approximates the continuum. In our use of this formula, we always check to see that this assumption is correct.

The same formulation has been considered previously by Wolynes and co-workers [12]. Its advantages are two-fold: (i) From a single Monte Carlo trajectory, one obtains the correlation function for *all* real-time points t that are less than or equal to a maximum possible time τ. Separate calculations for each different t are not necessary. (ii) The cyclical structure of Eq. (2.3b) allows one to account for all possible constructive and destructive interferences simultaneously.

Since the bath is harmonic and its coupling to the two-level system is linear, the bath degrees of freedom can be integrated out exactly to yield an influence functional. This reduces Eq. (2.3b) to a sum over spin paths only

$$\langle h_A(0)h_A(t)\rangle = \frac{\sum_{\{\sigma\}} \exp(\Omega'[\sigma_1,\ldots,\sigma_{P+2Q}])h_A(\sigma)h_A(\sigma')}{\sum_{\{\sigma\}} \exp(\Omega'[\sigma_1,\ldots,\sigma_{P+2Q}])}, \tag{2.5}$$

where the reduced action is given by

$$\Omega'[\sigma_1,\ldots,\sigma_{P+2Q}] = \Omega_{\rm TLS}[\sigma_1,\ldots,\sigma_{P+2Q}] + \chi[\sigma_1,\ldots,\sigma_{P+2Q}] . \tag{2.6}$$

Here $\Omega_{\rm TLS}$ is the sum of three piecewise actions for the uncoupled two-level system and is given by the following equation, which is analogous to Eq. (2.4):

$$\begin{aligned}\Omega_{\rm TLS}[\sigma_1,\ldots,\sigma_{P+2Q}] = & S_{\rm TLS}[\sigma_1,\ldots,\sigma_{P+1};\beta\hbar] \\ & + S_{\rm TLS}[\sigma_{P+1},\ldots,\sigma_{P+Q+1};-i\tau] \\ & + S_{\rm TLS}[\sigma_{P+Q+1},\ldots,\sigma_1;i\tau] , \end{aligned} \tag{2.7}$$

where

$$S_{\rm TLS}[\sigma_1,\ldots,\sigma_{N+1};\gamma\hbar] = \tfrac{1}{2}\ln\left[\tanh\frac{\gamma K}{N}\right]\sum_{i=1}^{N}\sigma_i\sigma_{i+1} . \tag{2.8}$$

The influence functional

$$\chi[\sigma_1,\ldots,\sigma_{P+2Q}] = \sum_{i,j}\tfrac{1}{2}\sigma_i\chi_{ij}\sigma_j \tag{2.9}$$

contains nonlocal complex-valued two-spin couplings

$$\chi_{ij} = \frac{\hbar}{\pi}\Delta_i\Delta_j\int_0^\infty d\omega\, J(\omega)\frac{\cosh[\hbar\omega(\Delta_{ij}-\Delta_{ji})/2]}{\sinh(\beta\hbar\omega/2)} , \tag{2.10}$$

where the time discretization

$$\Delta_i = \begin{cases} \beta\hbar/P, & 1\leq i\leq P \\ i\tau/Q, & P+1\leq i\leq P+Q \\ -i\tau/Q, & P+Q+1\leq i\leq P+2Q \end{cases} \tag{2.11}$$

and

$$\Delta_{ij} \equiv \sum_{k=i}^{j-1}\Delta_k . \tag{2.12}$$

The reduced action defined in Eqs. (2.6), (2.8), and (2.9) can be represented more compactly as

$$\Omega' = \Omega_{\rm TLS} + \chi \equiv \sum_{ij}\tfrac{1}{2}\sigma_i M_{ij}\sigma_j . \tag{2.13}$$

The system defined by the reduced action Ω' in Eq. (2.13) is isomorphic to a one-dimensional Ising model with nonclassical couplings. The nearest-neighbor interactions may be either real or imaginary. The long-range couplings are in general complex valued. Due to these long-range interactions, the spin-boson model cannot in general be solved exactly. Moreover, Monte Carlo simulations of this isomorphic Ising model are difficult due to the presence of nonpositive definite "weights" that alternate in sign. In the following section, we will discuss methods to treat this alternating weights problem.

III. STATIONARY-PHASE FILTERING

This section serves as a brief review of the stationary-phase Monte Carlo method [23–25]. We follow closely the development of Doll and co-workers [24].

Functional integral encountered in quantum dynamics are generally characterized by a complex-valued action. As a result, the integrand is an oscillatory functional of the path. In discretized form, these dynamical functional integrals has the generic form

$$I = \int d^N x\, \rho[\mathbf{x}]e^{i\phi[\mathbf{x}]} , \tag{3.1}$$

where $\rho[\mathbf{x}]$ is a positive definite function and $\phi[\mathbf{x}]$ is real.

The most significant contribution to the integral in Eq. (3.1) comes from regions of configuration space where the phase $\phi[\mathbf{x}]$ is nearly stationary. Everywhere else, the rapid phase oscillations lead to destructive interference.

A successful scheme to compute the integral must therefore concentrate sampling near these stationary-phase regions. This is the idea behind the SPMC method.

A filtering function is used to isolate stationary-phase regions. Instead of computing Eq. (3.1) directly, one computes

$$I=\int d^N x\, D[\mathbf{x}]\rho[\mathbf{x}]e^{i\phi[\mathbf{x}]}\ , \tag{3.2}$$

with the filtering function

$$D[\mathbf{x}]\equiv\int d^N y\, P[\mathbf{y}]\left[\frac{\rho[\mathbf{x}-\mathbf{y}]}{\rho[\mathbf{x}]}\right]\times e^{i\phi[\mathbf{x}-\mathbf{y}]-i\phi[\mathbf{x}]}\Big/\int d^N y\, P[\mathbf{y}]\ , \tag{3.3}$$

and $P[\mathbf{y}]$ is an arbitrary normalizable probability. For the present application, the probability function $P[\mathbf{y}]=\exp(-\sum_j y_j^2/2\epsilon_j^2)$ suggested by Doll and co-workers is most convenient. The widths $\{\epsilon_j\}$ are chosen according to $\epsilon_j=\epsilon_0\Delta_j$, where Δ_j is the characteristic width of $\rho[\mathbf{x}]$ in the variable x_j [24].

In general, the exact analytical form of $D[\mathbf{x}]$ is unknown. Therefore it is necessary to approximate it by its first-order approximant

$$D[\mathbf{x}]\approx D^0[\mathbf{x}]\equiv\exp\left[-\tfrac{1}{2}\sum_j\epsilon_j^2\left[\frac{\partial\phi}{\partial x_j}\right]^2\right]\ , \tag{3.4}$$

which is positive definite. A significant feature of D^0 is that it emphasizes only those regions where the phase function ϕ is nearly stationary. The integration of Eq. (3.1) can then proceed by normal Monte Carlo sampling of

$$I=\int d^N x\, D^0[\mathbf{x}]\rho[\mathbf{x}]e^{i\phi[\mathbf{x}]}(1+\Delta D/D^0)\ , \tag{3.5}$$

where $\Delta D\equiv D-D^0$, using $D^0[\mathbf{x}]\rho[\mathbf{x}]$ as the weight. As has been pointed out by Doll and co-workers [24], the role of the filter D^0 is to "synthesize" the appropriate phase interference such that the regions of highly rapid phase oscillations contribute a negligible amount to the integral.

Care needs to be exercised when evaluating the correction factor $1+\Delta D/D^0$. Since D^0 is approximate, the correction factor may become very large and highly oscillatory away from the stationary-phase regions, where D^0 is small. In this case, an indiscriminate sampling of the correction factor will lead to serious phase oscillation problems. A logical solution to this problem has been discussed by Doll and co-workers [24]. They suggest that for regions where D^0 is small, the correction factor is unimportant due to the rapid phase oscillations there. Consequently, they proposed imposing a cutoff value D_c such that they only evaluate the correction factor for configurations with $D^0\geq D_c$. Doll and co-workers have shown in a number of cases that quite accurate results can be obtained even with $D_c=1$ (i.e., no correction).

As we will discuss shortly, this happy circumstance is not found in the spin-boson model unless the SPMC method is generalized. Before venturing into this issue, it is first necessary to reformulate the spin-boson system as a continuous model.

IV. HUBBARD-STRATONOVICH TRANSFORMATION

To recast the summations in Eq. (2.5) as integrals, we perform a Hubbard-Stratonovich transformation [29]. The first step is to construct a new action

$$\Omega''\equiv\sum_{i,j}\tfrac{1}{2}\sigma_i(M+A)_{ij}\sigma_j \tag{4.1}$$

from Ω' of Eq. (2.13), where A is an arbitrary diagonal matrix with elements $a_1,\ldots,a_{P+2Q}$. Note that replacing Ω' in Eq. (2.5) by Ω'' does not alter the validity of Eq. (2.5). We introduce Ω'' so that we can make use of the well-known Gaussian integral identity

$$\int d^N S\exp\left[-\tfrac{1}{2}\sum_{i,j}s_i(M+A)^{-1}_{ij}s_j+\sum_j\sigma_j s_j\right]=\exp\left[\tfrac{1}{2}\sum_{i,j}\sigma_i(M+A)_{ij}\sigma_j\right]\times\int d^N S\exp\left[-\tfrac{1}{2}\sum_{i,j}s_i(M+A)^{-1}_{ij}s_j\right]\ . \tag{4.2}$$

Making this substitution into Eq. (2.5), and summing over the spin configurations explicitly, one obtains an expression for $\langle h_A(0)h_A(t)\rangle$ in a continuum representation

$$\langle h_A(0)h_A(t)\rangle=\frac{\int\prod_{k=1}^{P+2Q}ds_k\, W[s_1,\ldots,s_{P+2Q}]h_A(s)h_A(s')}{\int\prod_{k=1}^{P+2Q}ds_k\, W[s_1,\ldots,s_{P+2Q}]}\ , \tag{4.3}$$

where

$$W[s_1,\ldots,s_{P+2Q}]\equiv\exp\left[-\tfrac{1}{2}\sum_{i,j}s_i[M+A]^{-1}_{ij}s_j+\sum_j\ln(2\cosh s_j)\right] \tag{4.4}$$

and

$$h_A(s)\equiv\frac{e^{-s}}{2\cosh s}\ . \tag{4.5}$$

This transformation is valid as long as $\mathrm{Re}(M+A)$ is positive definite. The matrix A has therefore been introduced into Eq. (4.1) to ensure that this condition is satisfied. In our application, we have chosen to let $A=a_0 I$, where I is the identity matrix (i.e., $a_1=a_2=\cdots\equiv a_0$) such that $A_0+\min_j\mathrm{Re}(\lambda_j)>0$, where λ_j are the eigenvalues of M.

Equation (4.3), with Eq. (4.4) and (4.5), is an *exact* transformation of the discrete Ising model with couplings $\frac{1}{2}(M+a_0 I)_{ij}$ to a continuous "spin" model with new couplings $-\frac{1}{2}(M+a_0 I)^{-1}_{ij}$. The Taylor expansion

$$-a_0^2(M+a_0 I)^{-1}=-a_0 I+M-a_0^{-1}M^2+\cdots \tag{4.6}$$

shows that the new continuous spin model has the same characteristics as the discrete model, provided that a_0 is

large enough. The transformation of this type is known as a Hubbard-Stratonovich transformation [29]. Now, we may consider treating Eq. (4.3) with the SPMC method described in Sec. III.

V. CONTOUR DISTORTION

As has been discussed in Sec. III. the major role of the SPMC method is to seek out stationary paths in real space, and concentrate sampling around them. In order to understand the utility and limitation of the SPMC method, it is necessary to analyze the nature of these stationary paths. We will show in this section that a straightforward application of SPMC is inadequate for our current problem, and it has to be supplemented by contour distortion techniques.

According to Hamilton's least action principle, the stationary paths of the action would correspond to the *classical* paths. In a system dominated by tunneling, such as in the spin-boson model, such classical paths do not exist, at least not in real space and/or real time [30,31]. Consequently, if stationary paths do exist, they must not be confined to real space and/or real time.

At this point, our discussion may be made more concrete by turning to the discretized form of the action. After discretization of the action, space-time paths are parametrized by a point in multidimensional space (and specifically in our case, this space has dimension $P+2Q$). The stationary *paths* are now mapped onto stationary *points* in this multidimensional space, and for this discretized action, we may reach a conclusion similar to the one we made in the preceding paragraph: If stationary points in this multidimensional space do exist, they must be complex valued.

The appropriate way to handle complex-valued stationary point is familiar in semiclassical approximations [31,32]. The integration contour is distorted to pass through the stationary point, and then the steepest-descent method is applied. The theory behind such approaches is an elementary subject in the study of complex variables. For any integral of a function of a single complex variable, the steepest-descent trajectory emanating from a stationary point is uniquely defined. For example, the integral

$$I=\int_C dz\, g(z)\ , \tag{5.1}$$

whose original contour C lies entirely on the real axis, can be performed by passing a distorted contour C' along the steepest-descent direction through a stationary point z_0 in the complex plane, provided that $g(z)$ is analytic. C' is uniquely given for z_0. For every point $z\in C'$, the phase of the integrand $g(z)$ is constant. The sign problem is then completely eliminated by choosing the integration contour to be C'.

For multidimensional integrals like the one required by Eq. (4.3), the situation is quite different. Consider, for example the multidimensional integration

$$I^{(n)}=\int_{C_1} dz_1 \cdots \int_{C_n} dz_x g^{(n)}(z_1,\ldots,z_n)\ , \tag{5.2}$$

where $C_1,\ldots,C_n$ denote contours along the real axis and $g^{(n)}$ is an analytic function of n complex variables in the region that we are interested in. Any one of the contours of integration C_i may be distorted to a new complex-valued contour C_i', which itself must not be a function of $\{z_j: j\neq i\}$. In this way, we can distort the contours one after another to ensure that they intersect at any given stationary point in the n-dimensional complex space. However, since $\{C_j'\}$ must be chosen independently from each other, there exists no unique set $\{C_j'\}$ for which every point $\{z_1,\ldots,z_n\}\in\{C_j'\}$ satisfies the steepest-descent condition $\partial g^{(n)}(z_1,\ldots,z_n)/\partial z_j=0$, for all j simultaneously. Therefore one concludes that in more than one dimension, the sign problem can *never* be eliminated completely irrespective of the choice of the integration contours.

Another important question concerning the usefulness of contour distortion in many dimensions is related to the multiplicity of stationary points. If there exist a number of different stationary points in the multidimensional complex space, one should in principle seek a set of distorted contours $\{C_j'\}$ that contains as many stationary points as possible. In general, this is a difficult task because of the following two problems. (i) The first problem is a technical one: not all stationary points can be found explicitly. To circumvent this, Doll and co-workers suggested using simulated annealing techniques to find the approximate locations of stationary points [33]. In other instances, the approximate locations of stationary points can be found by numerical root finding methods. For the current problem, we have taken the second approach. (ii) Even after *all* stationary points have been found, a more serious conceptual problem remains: there exists no general algorithm to parametrize $\{C_j'\}$ such that it contains all or most of the stationary points. Therefore, in a practical application of contour distortion methods, one aims at finding a compromise between the following two factors: (a) to maximize the number of distinct stationary points connected by the distorted contours; (b) to keep the distortion simple to facilitate easy parametrization.

For the spin-boson problem, we have *neither* of the two general problems mentioned above, and we have taken a simple approach for determining the appropriate distortions. In our calculations, we distort the integration contour C_j in each of the n variables by simply rotating it into the complex plane through a constant angle θ_j. The rotation angles $\{\theta_j\}$ are determined so that the n distorted contours $\{C_j'\}$ intersect at a stationary point in the n-dimensional complex space. Details of how the stationary points are located and why our simple method works are left to Appendix A.

Similar contour rotations have been considered before [26], but the reasoning and applications are significantly different. The usefulness of these contour distortions will be demonstrated in Sec. VII where SPMC calculations in some exactly solvable limits are compared with analytical results.

VI. GENERALIZED STATIONARY-PHASE MONTE CARLO ALGORITHM

The computational problem is defined by Eqs. (4.3)–(4.5). Our approach consists of first distorting the

integration contours by simple rotations into the complex plane to increase the efficiency of the sampling, as described in Sec. V, and subsequently, using the SPMC method introduced in Sec. III to perform the multidimensional contour integrals.

After contour rotations, Eq. (4.3) becomes

$$\langle h_A(0)h_A(t)\rangle = \frac{\int \prod_{k=1}^{P+2Q} ds_k \tilde{W}[\mathbf{s}]\tilde{h}_A(s)\tilde{h}_A(s')}{\int \prod_{k=1}^{P+2Q} ds_k \tilde{W}[\mathbf{s}]} , \quad (6.1)$$

where $\mathbf{s}=\{s_1,\ldots,s_{P+2Q}\}$ and

$$\tilde{W}[\mathbf{s}]\equiv\exp\left[-\tfrac{1}{2}\sum_{i,j} s_i(1+i\tan\theta_i)(M+A)^{-1}_{ij} \times(1+i\tan\theta_j)s_j + \sum_j \ln[2\cosh(1+i\tan\theta_j)s_j]\right] , \quad (6.2)$$

where θ_j is the rotation angle for the jth variable, and

$$\tilde{h}_A(s_j)\equiv\frac{\exp[-(1+i\tan\theta_j)s_j]}{2\cosh(1+i\tan\theta_j)s_j} =\exp\{-(1+i\tan\theta_j)s_j -\ln[2\cosh(1+i\tan\theta_j)s_j]\} . \quad (6.3)$$

For the integral in the denominator of Eq. (6.1), we define the "weight function"

$$\rho_d[\mathbf{s}]\equiv\exp(\mathrm{Re}\tilde{W}[\mathbf{s}]) \quad (6.4)$$

and the "phase function"

$$\phi_d[\mathbf{s}]\equiv\mathrm{Im}\tilde{W}[\mathbf{s}] . \quad (6.5)$$

Following the development in Sec. III, the first-order approximate filtering function is

$$D_d^0[\mathbf{s}]\equiv\exp\left[-\tfrac{1}{2}\sum_j \epsilon_j^2\left(\frac{\partial\phi_d}{\partial s_j}\right)^2\right] , \quad (6.6)$$

so the integral is given approximately by

$$\int \prod_{k=1}^{P+2Q} ds_k \rho_d[\mathbf{s}]e^{i\phi_d[\mathbf{s}]}D_d^0[\mathbf{s}] . \quad (6.7)$$

Performing a similar breakup of the integrand in the numerator of Eq. (6.1) yields a different weight function ρ_n and phase function ϕ_n, therefore resulting also in a different filtering function D_n^0. This is cumbersome. We prefer to use the same weight function and filtering function for both the numerator and the denominator:

$$\langle h_A(0)h_A(t)\rangle \approx\frac{\int \prod_{k=1}^{P+2Q} ds_k \rho_d[\mathbf{s}]D_d^0[\mathbf{s}]\left[\frac{\rho_n[\mathbf{s}]D_n^0[\mathbf{s}]}{\rho_d[\mathbf{s}]D_d^0[\mathbf{s}]}\right]e^{i\phi_n[\mathbf{s}]}}{\int \prod_{k=1}^{P+2Q} ds_k \rho_d[\mathbf{s}]D_d^0[\mathbf{s}]e^{i\phi_d[\mathbf{s}]}} , \quad (6.8)$$

so $\rho_d[\mathbf{s}]D_d^0[\mathbf{s}]$ can be used as the sampling function for a Monte Carlo integration. The error in Eq. (6.8) can be estimated by computing the correction factor $(1+\Delta D/D^0)$, as in Eq. (3.5).

At this point, the Monte Carlo sampling should proceed in a straightforward manner. Using the standard Metropolis algorithm [34], we have attempted to perform the sampling in Eq. (6.8). Unfortunately, this simple sampling scheme when applied to the present problem displayed extremely slow equilibration rate, much like a system close to its critical point. Such a problem is not entirely surprising because the spin-boson Hamiltonian has a bistable structure, analogous to ϕ^4 field theory. The isomorphic Ising model does, of course, have long-ranged interactions. But this is not the primary source of the slowing down in our calculations. It is the result of the filtering functions D^0, which introduces highly nonlocal interactions between distant sites along the ring. Its physical origin is that regions of configuration space where the action is nearly stationary are well separated from each other. In order to make transits among these stationary regions, massive global rearrangements of the system configuration have to be effected.

To circumvent the slow equilibration problem, we have incorporated several special types of Monte Carlo moves into our program. We will briefly describe here each kind of Monte Carlo move we have employed.

(1) Simple Metropolis: Single particle moves of maximum step size Δ_{SM} in random directions are made and accepted or rejected using the Metropolis criterion. Δ_{SM} is less than the separation between the two stable wells, so simple Metropolis equilibrates the system within each well, but rarely results in transits between the two wells.

(2) Kink Metropolis: To supplement the simple Metropolis steps, kink-forming Metropolis moves were performed by reflecting (or "flipping") each particle across the origin, one at a time. This allows transits from one well to the other (hence the name "kink forming").

(3) Kink-pair-forming Metropolis: Under high coupling to a reasonably fast-responding bath, influence functional bonds produce strong correlations between pairs of particles from the forward and reverse time paths. Hence kinks form predominantly in pairs. The kink-pair-forming Metropolis move is designed to enhance such correlated motions.

(4) Swendsen-Wang: This type of motion is conceptually similar to the embedded dynamics of ϕ^4 theory discussed by Brower and Tamayo [35], based on the Swendsen-Wang method [36–38]. This method identifies the boundaries between strongly correlated blocks which are not necessarily contiguous. The correlated blocks are flipped independently. This algorithm is extremely effective in producing long-range correlated kinks. Further discussion of this method as applied to the current problem is given in Appendix B.

In each pass, steps (1) and (2) are attempted for every particle once on the average, step (3) is attempted for every possible pair once on the average, and step (4) is performed once for the entire system. Typical results presented in this paper were obtained using three to ten million Monte Carlo passes. Parts of the calculations

TABLE I. Summary of simulation results for $C(t)$ in various regions on the T-α plane.

$\alpha \leq 0.064$	$T/K=10$	$K/\omega_c=0.4$	Damped coherent oscillations
$\alpha \leq 0.064$	$T/K=7.5$	$K/\omega_c=0.4$	
$\alpha \leq 0.13$	$T/K=5$	$K/\omega_c=0.4$	
$\alpha \leq 0.32$	$T/K=2.5$	$K/\omega_c=0.4$	
$\alpha \leq 0.51$	$T/K=0.625$	$K/\omega_c=0.4$	
$\alpha \leq 2.55$	$T/K=0.625$	$K/\omega_c=1.6$	Coherent oscillations similar to adiabatic limit
$\alpha=1.27$	$0.5 \leq T/K \leq 1.2$	$K/\omega_c=0.1$	Exponential relaxation with time constant $\tau \simeq T^{-1.6}$ following short-time transient
$\alpha=2.55$	$0.625 \leq T/K \leq 2.5$	$K/\omega_c=0.4$	Exponential relaxation with time constant $\tau \simeq e^{-0.056K/T}$
$\alpha=0.64$	$0.625 \leq T/K \leq 15$	$K/\omega_c=0.4$	Short time exponential decay with time constant $\tau \simeq T^{0.4}$ followed by long-time tail

were performed on the Cray X-MP at Berkeley, at the speed of approximately 1 CPU h per million passes. The rest of the calculations were performed on an IBM RISC/6000 Model 320, at about one-fifth the speed of the Cray X-MP.

VII. RESULTS AND DISCUSSION

This section presents the numerical results. In cases where exact solutions of the spin-boson problem are known, we compare our results with the exact or asymptotic solutions to demonstrate the quality of our computations. Then we discuss numerical results for parts of the parameter space where such solutions are not known. From these data, the coherent-incoherent boundary will be located and compared to the prediction of the noninteracting-blip approximation. The temperature dependence of the incoherent relaxation rate will be determined for high dissipations. Finally, we will present results for a region in the parameter space that is inaccessible to previous approximate analytical theories. Our major conclusions concerning the behavior of $C(t)$ for various regions on the T-α plane are summarized in Table I.

A. Comparison with exact results

In the limit of zero coupling to the bath, the dynamics of the isolated two-level system is easily solved. Perfect quantum coherence is maintained indefinitely, which is manifested in the cosine oscillations of the spin correlation function.

Figure 1(a) shows numerical results for the isolated two-level system with $T/K=(\beta K)^{-1}=2.5$ after contour rotations. We use units for temperature T where Boltzmann's constant is 1. The solid line represents the exact result. Vertical bars indicate error estimates of one standard deviation. In this case, discretizations of $P=2$ and $Q=16$ were used. Convergence was verified by recomputing the correlation functions using finer discretizations of $P=4$ and $Q=32$, which yielded similar results. A SPMC width of $\epsilon_0=0.3$ was chosen and the re-

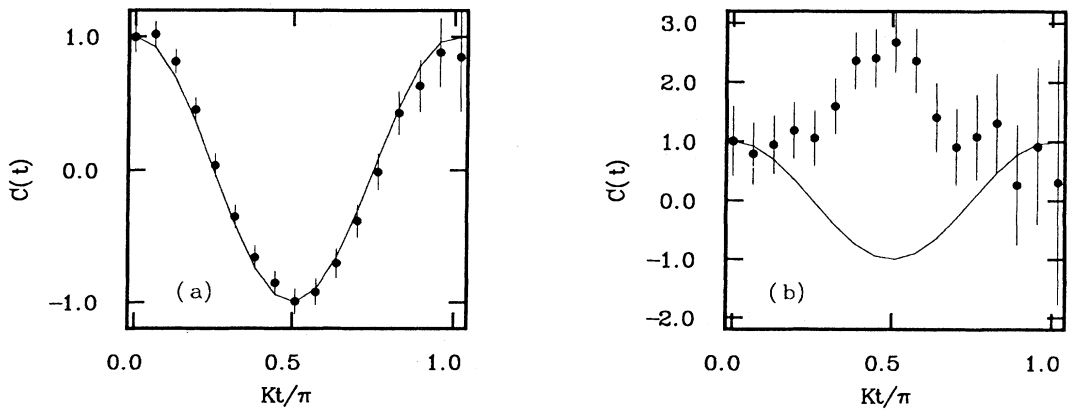

FIG. 1. Numerical results for $C(t)$ at $T/K=2.5$ with coupling $\alpha=0$ computed using the SPMC method (a) after rotations and (b) with no rotations. Vertical bars indicate error estimates of one standard deviation. Solid curves are exact results.

sults were obtained *without* correcting for D_0. Figure 1(a) shows that the uncorrected results are quite accurate. Correcting for D_0 improved the results by about 5% on the average, but required substantially more computations. It is worth noticing that although the isolated two-level system is the most trivial case from an analytical standpoint, it presents the most nontrivial computational problem. As discussed in Appendix A, the isolated two-level system possesses an extremely large number of important stationary points. As a result, a very thorough equilibration is necessary to ensure that all the relevant configurations are sampled. This is in part facilitated by the Swendsen-Wang method. However, the efficiency of the sampling was still found to be rather slow. The data shown in Fig. 1(a) were generated from 8 million Monte Carlo passes, after 2 million equilibration passes, using a total of approximately 10 CPU h on the Cray X-MP.

The corresponding results using the same number of passes but with *no* contour rotations are shown in Fig. 1(b). Note that data obtained without contour rotations have much larger statistical error (the denominator actually has the incorrect sign [39].) As discussed in Sec. V, SPMC alone without contour distortions restricts integration paths to be classical and real valued. Tunneling in the spin-boson model is of course nonclassical, and therefore necessitates the inclusion of complex-valued paths.

The spin-boson problem is also exactly solvable in the adiabatic limit ($\omega_c \to 0$). In this case, the influence functional bonds in Eq. (2.9) produces infinitely long-range couplings and the isomorphic Ising model exhibits mean-field behavior [13], which can be analyzed as an elementary exercise [40]. The dynamics in this case exhibits coherence indefinitely [12–14]. Representative results in the adiabatic limit are presented in Fig. 2 for $T/K=2.5$ at different couplings. The numerical results compare favorably with analytical solutions.

B. Coherent-incoherent transition

At the zero-coupling limit, the isolated two-level system undergoes perfectly coherent dynamics. In the other limit of high coupling, the relaxation proceeds incoherently, in an exponential fashion [5]. For intermediate values of α, a transition from coherent to totally incoherent dynamics occurs, and the phase boundary for this transition has been predicted by the noninteracting-blip approximation [5]. According to that theory and what we find as well, the location of this coherent-incoherent transition is a strong function of temperature. The critical coupling α_c at which this transitions takes place shifts to higher values for lower temperatures.

To locate the coherent-incoherent boundary, we have computed spin correlation functions for many different points on the T-α plane. Representative numerical results for $K/\omega_c=0.4$ and a wide variety of temperatures are shown in Figs. 3–6. We use units for frequency ω, where $\hbar$ is 1. The results in these figures demonstrate that for large α, relaxation proceeds incoherently and the value of $C(t)$ approaches zero monotonically. On the other hand, for small α, the correlation function oscillates around zero and displays remnants of coherent dynamics. At some critical coupling α_c, coherence is completely quenched, and the system relaxes in a purely incoherent fashion. This critical coupling α_c shifts to larger values for lower temperatures.

The results of our calculations are summarized in Fig. 7, which reveals the location the coherent-incoherent transition boundary on the T-α plane. Open diamonds

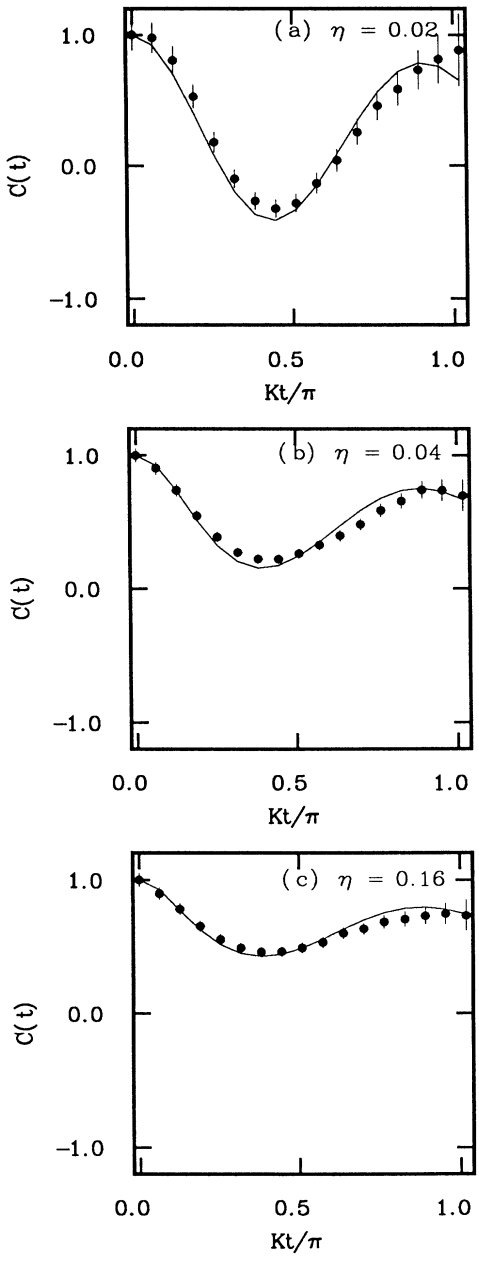

FIG. 2. Comparison of numerical data for $C(t)$ with exact analytical results for adiabatic limit $\omega_c \to 0$ at $T/K=2.5$ for three different couplings. Solid curves indicate exact results. Vertical bars denote error estimates.

denote spin correlation functions that exhibit purely incoherent relaxation and solid circles denote correlation functions with coherence. The solid line indicates the transition boundary predicted by the noninteracting-blip approximation [5,10]. Our simulations and the noninteracting-blip approximation show a remarkable agreement, indicating that this approximate analytical theory yields very accurate prediction about the location of the coherent-incoherent transition, except at very low temperature. The question of low temperature will be addressed shortly.

The good agreement between simulations and the noninteracting-blip approximation is perhaps surprising. The noninteracting-blip approximation is strictly valid only when $K \ll \omega_c$. In our calculations, we have chosen a $K/\omega_c = 0.4$, for which the noninteracting-blip approximation may no longer be applicable. Indeed, when we performed the calculations again at $K/\omega_c = 1.6$, the data, shown in Fig. 8, show that the spin-boson system now displays behaviors similar to the adiabatic limit. Figure

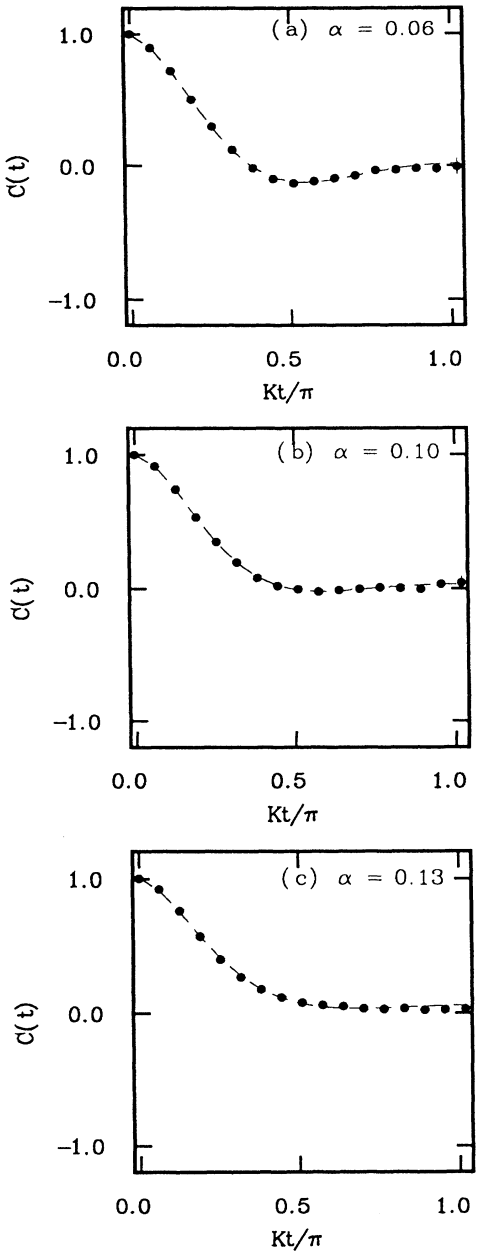

FIG. 3. Representative numerical results of $C(t)$ for $T/K = 10$ and $K/\omega_c = 0.4$ at three different values of α. (a) shows weak coherence and (c) shows purely incoherent relaxation. Vertical bars denote error estimates. Dashed lines are guides to the eye.

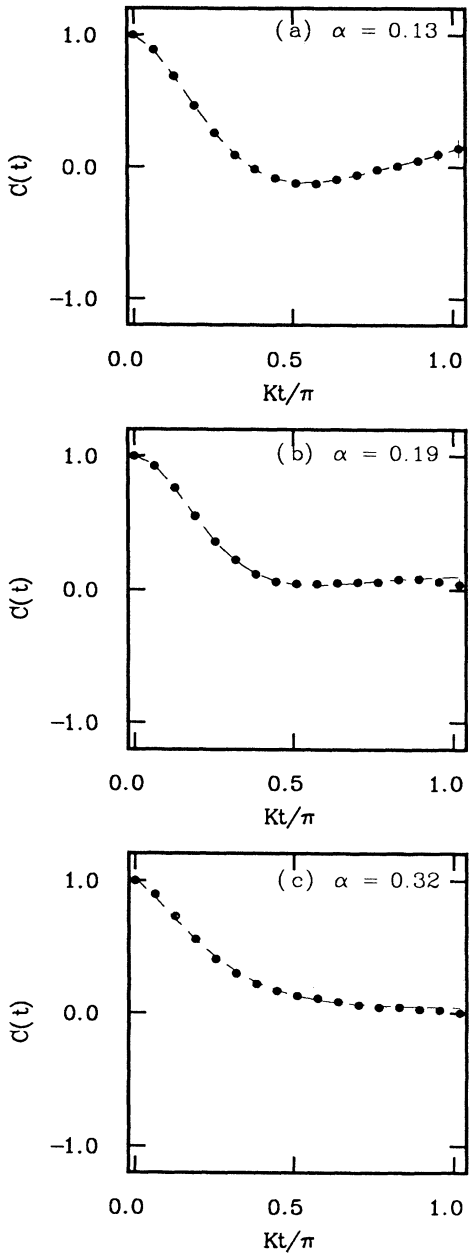

FIG. 4. Same as Fig. 3, for $T/K = 5$ and $K/\omega_c = 0.4$.

8(c) demonstrates that coherence remains even at an extremely large coupling of $\alpha=2.55$. The location of the coherent-incoherent boundary as predicted by the noninteracting-blip approximation is apparently a weak function of ω_c [10], as long as ω_c is not too small compared to K.

A last point concerning the legitimacy of the comparison between results from simulations and the noninteracting-blip approximation needs to be addressed, although it is not central to the results reported here. The noninteracting-blip approximation was originally developed to calculate the expectation value of σ at time t, with the initial condition that $\sigma(0)=+1$. This expectation value is often called $P(t)$ in the literature. Because σ_z is a nonlinear operator, $P(t)\neq C(t)$. However, this difference is expected to be small for the cases we have considered where $T/K\simeq O(1)$. An extension of the noninteracting-blip approximation to compute $C(t)$ directly has recently been formulated [41]. These workers show that deviations between $P(t)$ and $C(t)$ are most pronounced at very long times, which we have not focused on in this work. See below, however.

The fact that we have considered the noninteracting-blip approximation for $P(t)$ rather than $C(t)$ changes the

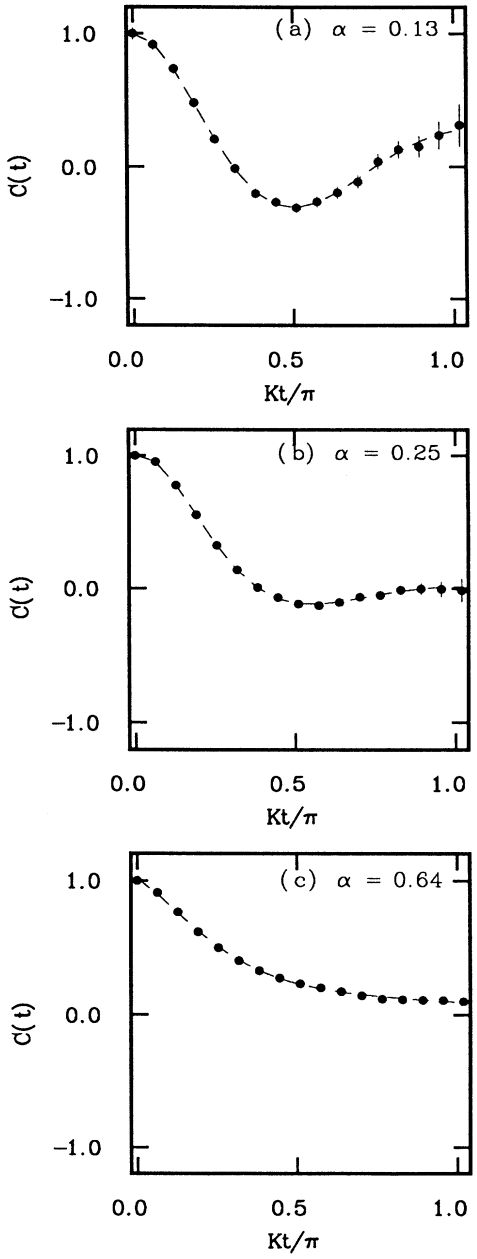

FIG. 5. Same as Fig. 3, for $T/K=2.5$ and $K/\omega_c=0.4$.

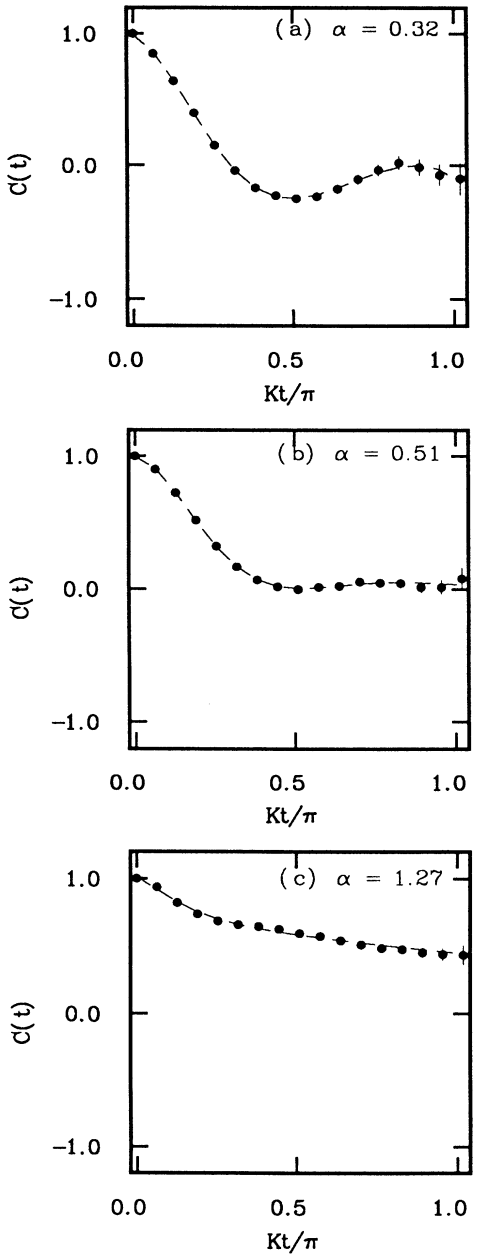

FIG. 6. Same as Fig. 3, for $T/K=0.625$ and $K/\omega_c=0.4$.

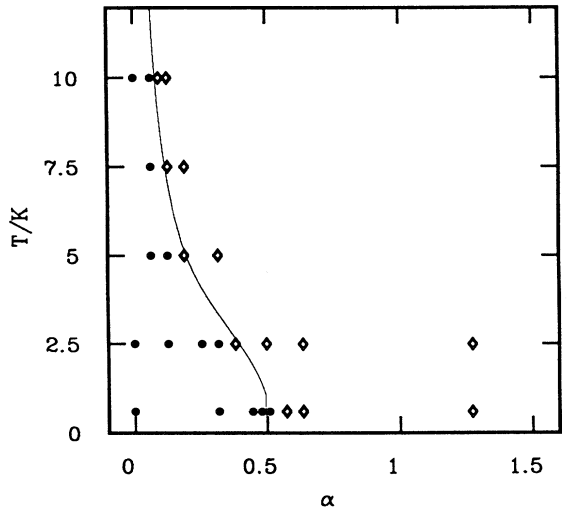

FIG. 7. Phase boundary for coherent-incoherent transition on the T-α plane. Open diamonds indicate purely incoherent relaxation. Solid circles indicate coherent behavior. Solid line is the coherent-incoherent boundary predicted by the noninteracting-blip approximation [5]. Note that for low temperatures, the actual phase boundary extends beyond $\alpha=0.5$.

picture only slightly. As shown in Fig. 7, the noninteracting-blip approximation concludes that the dynamics of the spin-boson model is purely incoherent above $\alpha=0.5$, for any temperature. However, the numerical results suggest that this is not true for $T/K=0.625$. The coherent-incoherent boundary appears to extend beyond $\alpha=0.5$ as the temperature continues to be lowered. Our simulation results corroborate with a previous study investigating the qualitative difference between $C(t)$ and $P(t)$ for $\alpha=0.5$ in the low temperature limit [41]. It was found that for long times, $C(t)$ approaches zero from *below,* indicating the phase boundary extents beyond $\alpha=0.5$ at low temperatures.

This is an appropriate place to comment briefly on the difference between $C(t)$ and $P(t)$. The simulation results we have presented up to this point are for $C(t)$. But we have also computed $P(t)$ over the entire T-α plane, by constraining the spins on the thermal path to have the same sign in the simulations. In Figs. 9 and 10, we compare results for $P(t)$ to $C(t)$ at two different temperatures for various values of α. Our results show that $P(t)$ and $C(t)$ are qualitatively similar at all of the temperatures we have studied ($T/K\geq 0.625$). The small, though observable, quantitative differences between $P(t)$ and $C(t)$ are more apparent at lower temperatures, in agreement with predictions from previous analytical theory [41].

Also of interest here is a quantitative comparison between the results of the simulations and of the noninteracting-blip approximation. The solid lines in Figs. 9 and 10 are results from the noninteracting-blip approximation. In both sets of figures, we have chosen three different values of α—one inside the coherent region, one near the coherent-incoherent phase boundary, and the last one in the incoherent region. For the reasons discussed above, the quantitative comparison between simulations results (using $K/\omega_c=0.4$) and the noninteracting-blip approximation (assuming $K/\omega_c\simeq 0$) is not expected to be very favorable, as is seen in Figs. 9 and 10. However, the noninteracting-blip approximation is remarkably accurate in reproducing the gross features of the correlation functions. This is primarily the reason

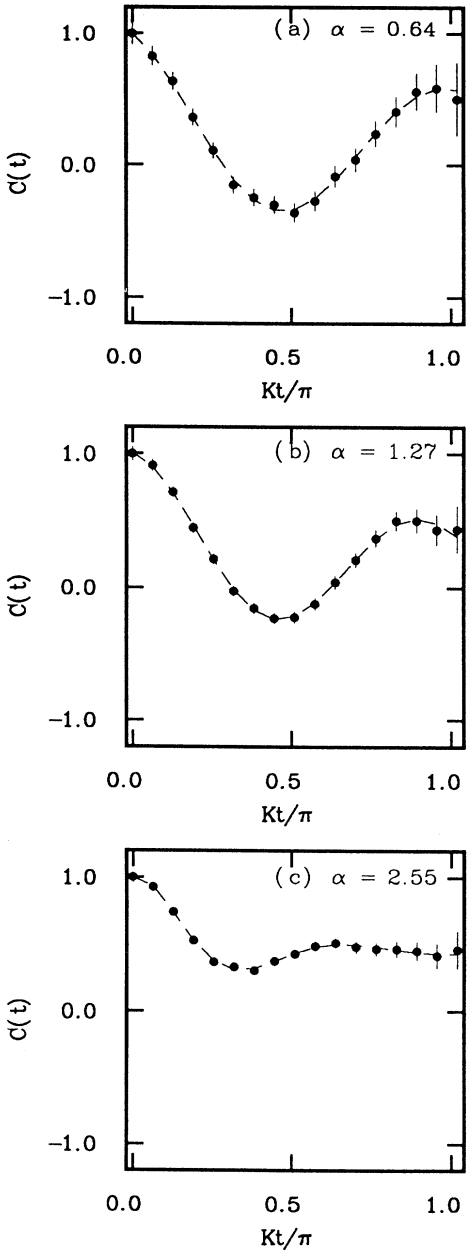

FIG. 8. Same as Fig. 6, also for $T/K=0.625$, but $K/\omega_c=1.6$. The coherence persists up to $\alpha\gg 0.5$, the critical coupling predicted by the noninteracting-blip approximation. This behavior is similar to the adiabatic limit, in which the noninteracting-blip approximation is not applicable. Dashed line are guides to the eye.

why the noninteracting-blip approximation is able to predict the location of the phase boundary with such a high precision (see Fig. 7), even for cases where ω_c is not rigorously large compared to K.

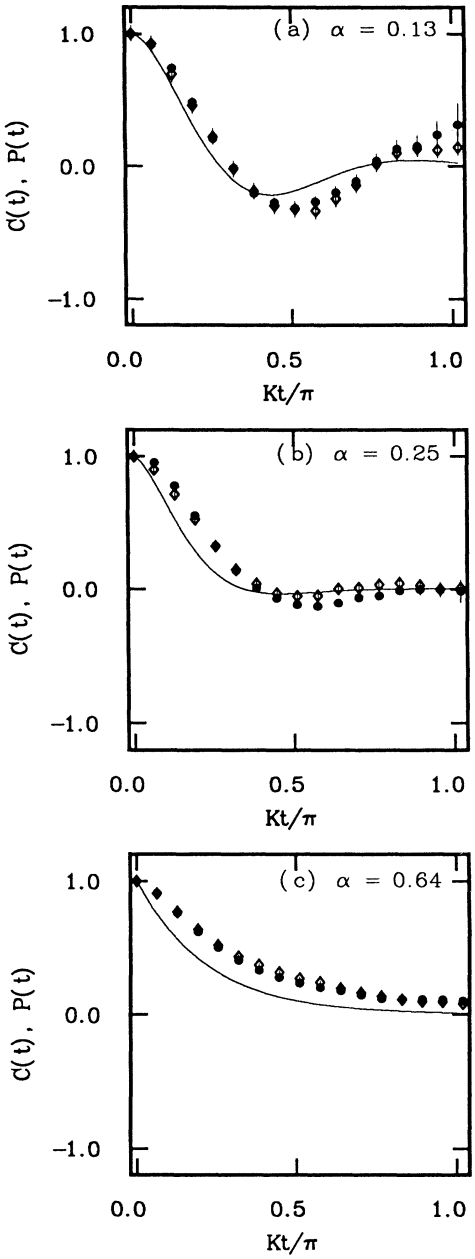

FIG. 9. Comparison of simulation results for $P(t)$ (diamonds) and $C(t)$ (circles), and predictions of the noninteracting-blip approximation (solid lines). $T/K=2.5$ and $K/\omega_c=0.4$. $P(t)$ and $C(t)$ show qualitatively similar behaviors. The noninteracting-blip approximation reproduces the gross features of $P(t)$ and $C(t)$ well: (a) inside the coherent region; (b) near the coherent-incoherent phase boundary, and (c) in the incoherent region.

C. Incoherent relaxation rates

Under high coupling, the spin correlation function relaxes exponentially. The temperature dependence of this exponential decay time constant can be extracted from the numerical data. Figure 11 shows typical relaxation behaviors at three different temperatures for $\alpha=1.27$ with $K/\omega_c=0.1$. After a short initial transient, relaxation at all temperatures proceed exponentially in the form $C(t)\simeq\exp(-t/\tau)$. The relaxation times are given in Table II, and as expected, they increase with the inverse temperature β. Figure 12 illustrates the variation of the

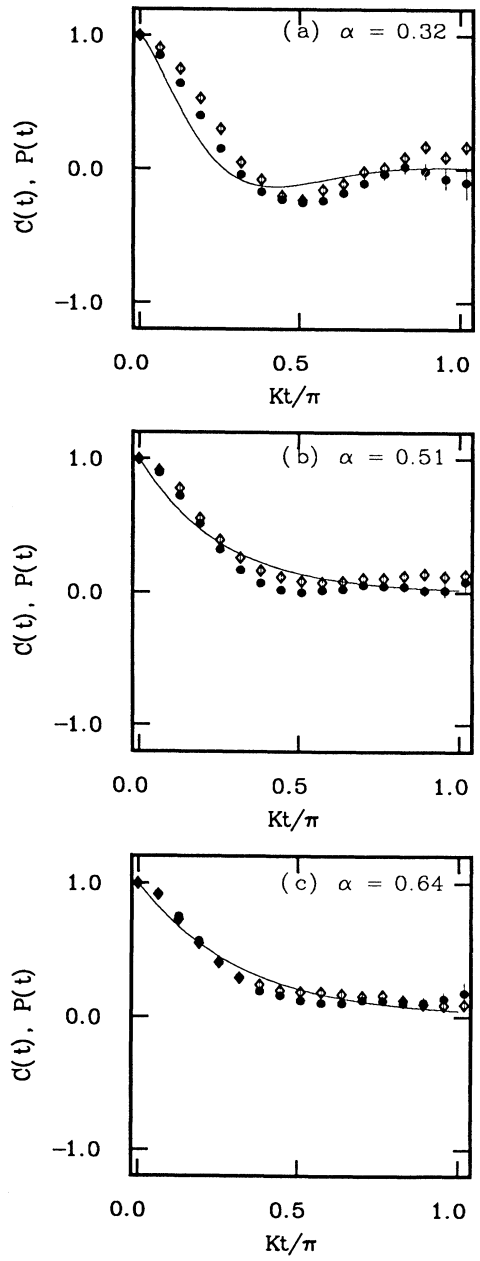

FIG. 10. Same as Fig. 9, for $T/K=0.625$ and $K/\omega_c=0.4$.

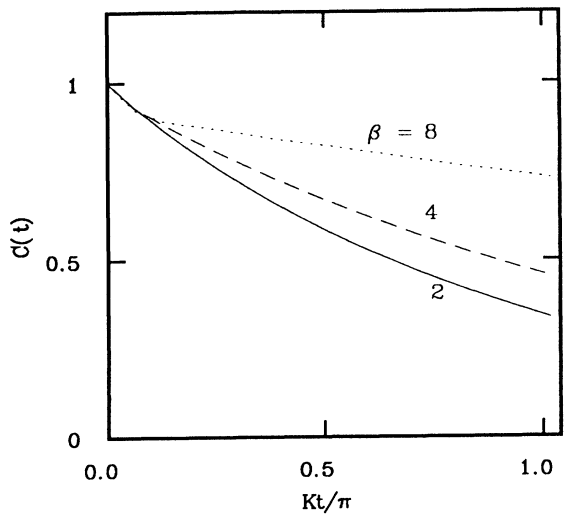

FIG.11. Relaxation of the spin correlation function in the deep-tunneling regime, for $\alpha=1.27$ and $K/\omega_c=0.1$ at three different temperatures. Following a short initial transient, they all exhibit exponential relaxation.

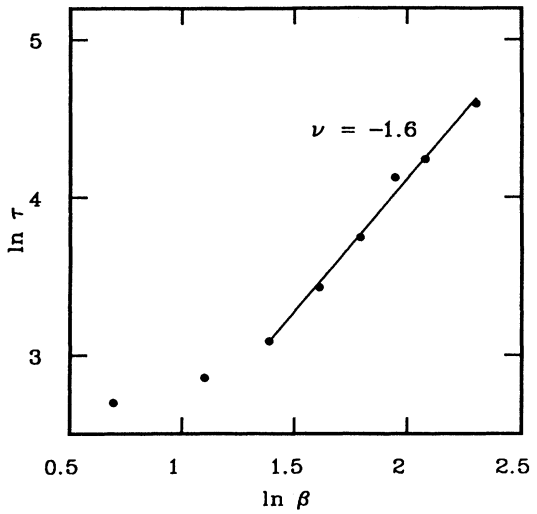

FIG. 12. Relaxation time constant in the deep-tunneling regime as a function of inverse temperature from Table II. $K/\omega_c=0.1$. The numerical result suggest that the temperature dependence of τ is given by a power law $\tau\sim T^{\nu}$, with $\nu\approx-1.6$ indicated by the straight line. Notice that the high-temperature data do not follow this power-law behavior.

relaxation time τ with inverse temperature β, on a log-log plot. At the low-temperature end, the relaxation time is observed to follow a power-law behavior $\tau\simeq T^{\nu}$, with $\nu\approx-1.6$.

In this so-called "deep-tunneling" regime, the relaxation rate can be calculated using the golden rule of time-dependent perturbation theory [5,15,16]. The predominant relaxation mechanism here is tunneling of the bath. In this regime, the golden rule and the noninteracting-blip approximation predict a non-Arrhenius temperature dependence for τ, with a power-law form $\tau\simeq T^{\nu}$ and exponent $\nu=1-2\alpha$. For $\alpha=1.27$, this yields a value for $\nu=-1.54$. This prediction from perturbation theory is in excellent agreement with the numerical results, as shown in Fig. 12.

Figure 12 also shows that at higher temperatures, the power-law breaks down. This is because tunneling is overtaken by classical activated processes. For a slow bath with a small ω_c, activated processes are especially prevalent. To illustrate this, we have performed another set of calculations using a slower bath ($K/\omega_c=0.4$) and higher coupling ($\alpha=2.55$). The relaxation times are shown in Fig. 13. For a temperature range similar to the previous set of results, the relaxation times in this case show purely Arrhenius temperature dependence with $\tau\simeq\exp(-\epsilon/T)$. Indeed, in the adiabatic limit of an infinitely slow bath where $\omega_c\to0$, we expect Arrhenius temperature dependence on the basis of standard analytical theory [7,14,42].

Finally, we investigate the relaxation behavior of the spin-boson system at intermediate coupling ($\frac{1}{2}<\alpha<1$) and low temperatures. This is the region in the T-α plane where the noninteracting-blip approximation is not expected to give accurate results. Consequently, the be-

TABLE II. Time constant τ for short-time exponential decay of $C(t)$ in the deep-tunneling regime. $\alpha=1.27$, $K/\omega_c=0.1$.

T/K	$\tau K/\pi$
2.5	0.94
1.7	1.10
1.2	1.40
1.0	1.97
0.83	2.70
0.71	3.93
0.62	4.42
0.50	6.28

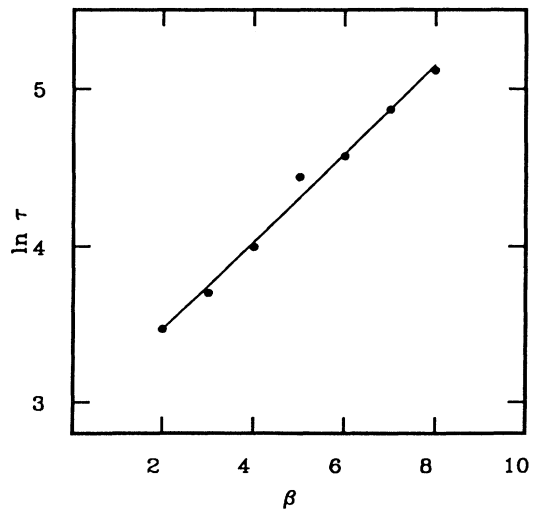

FIG. 13. Relaxation time constant in the semiclassical regime with $\alpha=2.55$ and $K/\omega_c=0.4$ follows Arrhenius behavior. Activated processes are overtaking tunneling.

havior of the spin-boson problem in this part of the parameter space is least understood. This is also the region in which the spin-boson model is most relevant to the Kondo problem [5]. The relaxation in this region has been assumed to be incoherent by previous approximate analytical theories.

We have computed the spin correlation function at $\alpha=0.64$ for a number of different temperatures. Some representative results are shown in Fig. 14. After a short transient, the spin correlation function exhibits exponential relaxation. For lower temperatures, however, this exponential relaxation is followed by a long-time tail of the power-law type $C(t)\simeq t^{x}$. Unfortunately, the quality of the numerical results at long time and low temperatures does not permit an accurate determination of this exponent. Despite this, the short-time exponential relaxation can be well characterized by a relaxation time τ. The relaxation times are given in Table III and plotted in Fig. 15 as a function of β on a log-log plot. Again, τ follows a power-law-type temperature dependence with $\tau\simeq T^{\delta}$. But in this region, τ displays an *inverse* temperature dependence, showing a positive but weak exponent $\delta\approx 0.4$. This indicates that the short-time exponential relaxation is *faster* for *lower* temperatures, a fact which we believe has not yet been predicted based on previous analytical theories.

TABLE III. Time constant τ for short-time exponential decay of $C(t)$ in the region $\frac{1}{2}<\alpha<1$. $\alpha=0.64$, $K/\omega_c=0.4$.

T/K	$\tau K/\pi$
0.625	0.220
1.25	0.273
1.87	0.340
2.50	0.373
3.75	0.464
5.00	0.510
7.50	0.560
10.0	0.654
15.0	0.865

VIII. CONCLUSIONS

We have presented in detail a general approach to simulate quantum dynamics based on discretized path-integral techniques. Our method combines stationary-phase Monte Carlo sampling and contour distortions to achieve high sampling efficiency. Contour distortions in the form of simple rotations have been chosen for convenience in the present study. To make frequent transits among widely separated stationary regions, a number of special Monte Carlo moves have to be incorporated. From the numerical results, we confirmed that using this simple approach, dynamics of tunneling systems in condensed phase can be simulated to long times.

When this method is applied to study the coherent-incoherent transition of the spin-boson model, we found that the coherent-incoherent boundary on the T-α plane is well predicted by the noninteracting-blip approximation. However, the critical coupling α_c at which crossover to incoherence occurs is a strong function of the bath cutoff frequency ω_c and the temperature T.

The relaxation of the spin correlation function at high coupling and low temperature is exponential in time. The temperature dependence of the relaxation time constant τ assumes a power-law form due to tunneling of the

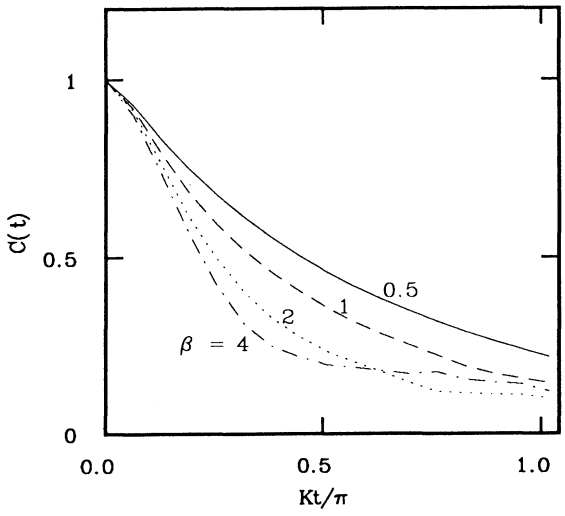

FIG. 14. Relaxation of the spin correlation function in the intermediate-coupling, low-temperature region, for $\alpha=0.64$ and $K/\omega_c=0.4$ at four different temperatures. The initial decay is exponential, followed by a slowly decaying incoherent background of the power-law type.

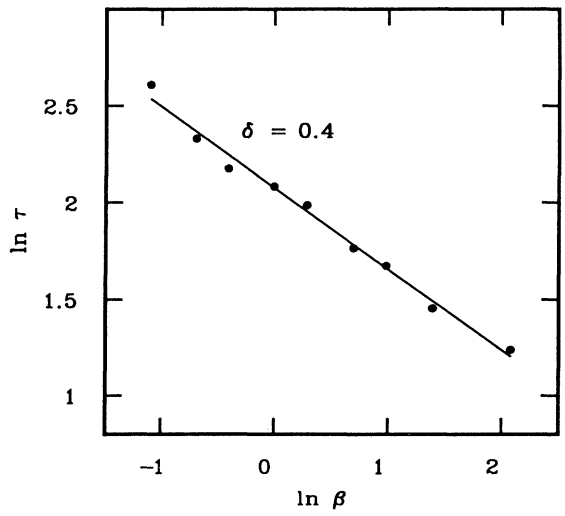

FIG. 15. Temperature dependence of the short-time relaxation time constant in the intermediate-coupling, low-temperature region (from Table III). $K/\omega_c=0.4$. The numerical results revealed an *inverse* power-law temperature dependence $\tau\sim T^{\delta}$, with the relaxation rate increasing with decreasing temperature, having a weak exponent $\delta\approx 0.4$, indicated by the straight line.

bath. This general behavior is well understood by the golden rule. At higher temperature and slower bath cutoff frequency ω_c, the power-law behavior is overtaken by an Arrhenius-type temperature dependence, reflecting the onset of classical activated processes.

In the intermediate coupling region $\frac{1}{2}<\alpha<1$, the relaxation of the spin correlation functions exhibits a short-time exponential behavior, followed by a long-time tail of the power-law type. The short-time exponential relaxation time constant shows a peculiar *inverse* temperature dependence, with the relaxation rate increasing towards lower temperatures. The relaxation time follows a power-law temperature dependence, with a weak exponent.

We believe that the general method that we have presented may provide a practical approach to solving the "sign problem" in many other contexts besides the spin-boson model. Whether our optimism is well founded must await further research on other quantum problems. Nevertheless, the success of the method we have described in this paper is evident in the great variety of behaviors so accurately described in the numerical simulations.

ACKNOWLEDGMENTS

This research was supported by the National Science Foundation and the U.S. Army Research Office. Many of the calculations were carried out on the Cray X-MP at the University of California, Berkeley. The authors also gratefully acknowledge computational resources provided by the IBM Corporation. Throughout this work, we have benefited from many fruitful discussions with John Gehlen.

APPENDIX A: LOCATING STATIONARY POINTS

The contour rotations described in Sec. V transforms original integration contours along the real axes by distorting them so that the new contours extend into the complex plane, intersecting at a stationary point. In this appendix, we will show explicitly how numerical iteration methods can be used to locate these stationary points and why contour distortions in the form of simple rotations are sufficient.

A stationary point denoted by the n-component vector $\mathbf{s}$ of Eq. (4.4) is given by the stationarity condition

$$-\sum_j (M+a_0 I)^{-1}_{ij} s_j + \tanh(s_i) = 0 \ , \tag{A1}$$

where $(M+a_0 I)$ is an $n\times n$ complex-valued matrix, and $\mathbf{s}$ is in general complex. (More than one such stationary point may exist.) First, we assume that $\mathrm{Re}(s_i) \gg \mathrm{Im}(s_i)$ for all i so that $\tanh(s_i)\approx\pm 1$. This may be used as the initial guess in an iterative process

$$(M+a_0 I)^{-1}\mathbf{s}^{(k+1)} = \mathbf{b}^{(k)} \ , \tag{A2}$$

with $\mathbf{b}^{(0)} \equiv (\sigma_1, \sigma_2, \ldots, \sigma_n)$ where σ_i is either $+1$ or -1 for each i. The iteration proceeds by taking

$$b_i^{(k+1)} = \tanh s_i^{(k+1)} \ . \tag{A3}$$

Obviously, the first iteration yields

$$s_i^{(1)} = \sum_j \sigma_j (M+a_0 I)_{ij} \ . \tag{A4}$$

Accordingly, our assumption that $\mathrm{Re}(s_i) \gg \mathrm{Im}(s_i)$ is valid as long as the value of a_0 is large enough.

The iterative process defined by Eqs. (A2) and (A3) converges to a different stationary point from every distinct initial guess $\mathbf{b}^{(0)}$. All stationary points can thus be generated by varying the numbers of $+1$ and -1 in $\mathbf{b}^{(0)}$ and then permuting the order of their appearance. It can easily be shown that the maximum number of distinct stationary points is

$$\sum_{k=0}^{n} \frac{n!}{k!(n-k)!} = 2^n \ .$$

After all stationary points have been located, the next step is to choose the appropriate contour distortions in such a way that the new contours will pass through all the stationary points. To parametrize one single set of distortions that accomplishes this is obviously prohibitive. The next best is to select contour distortions that pass through or near as many stationary points as possible, while keeping the form of distortions simple. In Sec. V, we suggest rotating the integration contours into the complex plane for each i such that the rotation angle

$$\theta_i = \tan^{-1}(\mathrm{Im}s_i / \mathrm{Re}s_i) \ . \tag{A5}$$

The symmetry of Eq. (A1) implies that if $\mathbf{s}$ is a stationary point, so is $-\mathbf{s}$. Therefore the simple rotated contours described by Eq. (A5) automatically intersect a pair of stationary points.

To give an example of the locations of the stationary points and the corresponding rotations defined by Eq. (A5), consider the case of the isolated two level system at $\beta=2$ and $\tau=16$, with $P=2$ discretizations on the thermal path and $Q=16$ discretizations on each of the real-time paths. One of the stationary points is obtained by using an initial guess $\mathbf{b}^{(0)}$ with all $n=P+2Q$ elements equal to $+1$. Figures 16(b) and 16(c), respectively, depict the real and imaginary parts of the elements of the n vector $\mathbf{s}$ around the ring. The corresponding rotation angles $\{\theta_i\}$ are shown as the open diamonds on Fig. 17. Again, because of symmetry, this set of rotated contours intersect not only one, but two distinct stationary points.

A different stationary point can be obtained from an initial guess $\mathbf{b}^{(0)}$ with two kinks, as shown in Fig. 18(a). Again, the real and imaginary parts, respectively, of the resulting stationary point are depicted in Figs. 18(b) and 18(c). Note that now the real part of $\mathbf{s}$ also has two kinks, reflecting the choice of the initial guess. The corresponding rotation angles are shown as the closed circles in Fig. 17. Except for the two pairs of elements enclosing the two kinks, the rotation angles are exactly the same as the ones defined for our first stationary point, which has no kinks. Based on this observation, we may conclude that the distorted contours defined for the first stationary point with no kinks will pass *near* all the stationary points with two kinks, expect at a small number of locations.

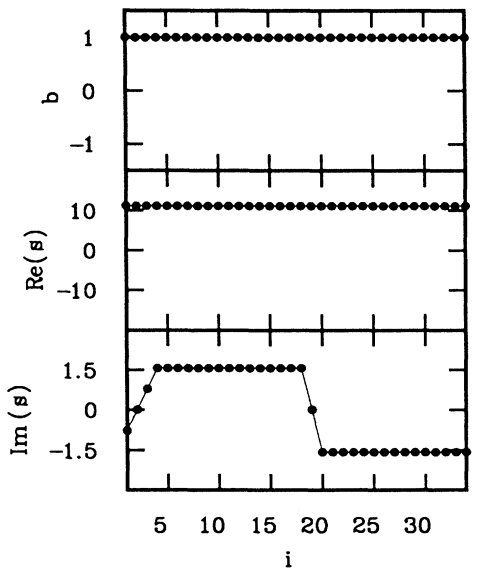

FIG. 16. Example of a stationary point obtained using the iterative procedure described in Appendix A, starting with an initial guess $\mathbf{b}^{(0)}$ with no kink, for $P=2$ and $Q=16$. The real and imaginary parts of the n vector $\mathbf{s}$ are plotted vs the index i along the ring. The thermal path begins at $i=1$ and ends at $i=3$. The forward time path begins at $i=3$ and ends at $i=19$. The reverse time path begins at $i=19$ and ends at $i=1$, where cyclic boundary condition applies.

Proceeding with the same analysis with stationary points of four kinks, six kinks, and so on, we observe that the rotations defined for the kinkless stationary point will pass *near* all other stationary points, as long as the number of kinks is not too large. Therefore, using the contour rotations defined by Eq. (A5) for the kinkless stationary point alone, we have accomplished the goal of choosing simple distortions that make a close approach with all other stationary points having a not too large number of kinks.

For the isolated two-level system which is uncoupled to the bath, we expect kink formation to be prevalent. Therefore the simple rotation scheme described above is likely not optimal. Indeed, our numerical results showed that the isolated two-level system, which possesses perfect quantum coherence, is the most difficult case to treat. As coupling to the bath increases, kink formation is suppressed, due to the influence functional bonds. Therefore, our simple rotation scheme will become better for higher couplings. The numerical data also agree with this anticipated result.

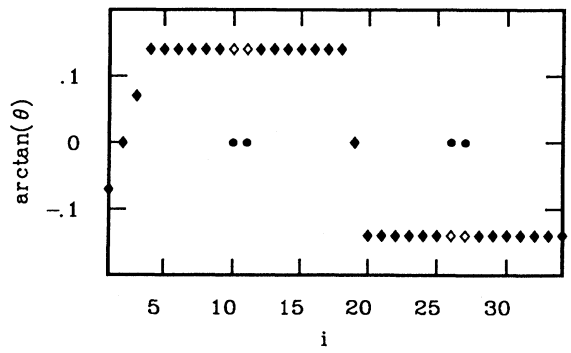

FIG. 17. The rotation angles corresponding to the stationary points in Fig. 16 (diamonds) and Fig. 18 (circles). Note that the two sets of rotation angles coincide at all but four points.

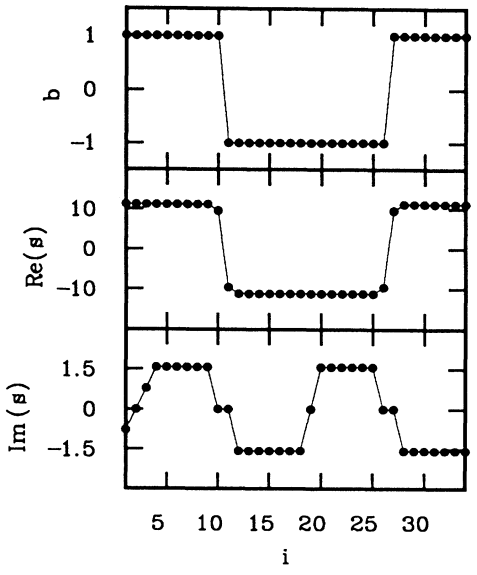

FIG. 18. Same as Fig. 16, for an initial guess $\mathbf{b}^{(0)}$ with two kinks.

APPENDIX B: EMBEDDED DYNAMICS WITH SWENDSON-WANG METHOD

In this appendix, the technical aspects of the Swendson-Wang method for the sampling of Eq. (6.8) will be discussed. The central idea is to embed discrete variables $\{\sigma_1,\ldots,\sigma_{P+2Q}\}$, which are responsible for the critical-like behavior, into the continuous fields $\{s_1,\ldots,s_{P+2Q}\}$. In a moment, we will discover that these embedded discrete variables behaves like spins, and they reflect whether the particle is in the left or the right well.

First, we replace the continuous variables by the following:

$$s_j=\sigma_j|s_j|\ , \tag{B1}$$

where $\sigma_j\equiv\mathrm{sgn}(s_j)$. Now consider freezing $\{|s_j|\}$ at their current values. It can easily be shown from Eqs. (6.4)–(6.6) that the weight function $\rho_d[\mathbf{s}]D_d^0[\mathbf{s}]$ in this reduced space takes on a bilinear exponential form in the $\{\sigma\}$ variables

$$\rho_d[\mathbf{s}]D_d^0[\mathbf{s}]\rightarrow\exp\left[\sum_{i,j}\sigma_i J_{ij}\sigma_j\right]\equiv\mathcal{P}[\sigma]\ , \tag{B2}$$

where $J_{ij}=J_{ij}[|s_1|,\ldots,|s_{P+2Q}|]$ is a function of the

frozen continuous fields. $\mathcal{P}[\sigma]$ is seen to be the distribution function for a one-dimensional Ising model with random (both ferromagnetic and antiferromagnetic) couplings.

A generalized Swendsen-Wang method has been formulated for Potts models [36–38]. Here we follow the development by Edwards and Sokal [38] and specializes to the Ising model. The probability distribution for an Ising model with random couplings J_{ij} is

$$\mathcal{P}[\sigma]=Z^{-1}\exp\left[\sum_{i,j}\sigma_i J_{ij}\sigma_j\right] \equiv\prod_{i,j}W_{ij}(\sigma_i,\sigma_j)\ , \tag{B3}$$

where $0\le W_{ij}(\sigma_i,\sigma_j)\le 1$ for every pair (i,j). We have specialized to the case

$$W_{ij}(\sigma_i,\sigma_j)=\begin{cases}\delta_{\sigma_i,\sigma_j}+w_{ij}(1-\delta_{\sigma_i,\sigma_j}) & \\ \qquad\qquad \text{if } J_{ij}\ge 0 \quad \text{(ferromagnetic)} & \\ w_{ij}\delta_{\sigma_i,\sigma_j}+(1-\delta_{\sigma_i,\sigma_j}) & \\ \qquad\qquad \text{otherwise} \quad \text{(antiferromagnetic)}\ , & \end{cases} \tag{B4}$$

where $w_{ij}\equiv\exp(-2|J_{ij}|)\ge 0$. Now define a conditional probability for a set of auxiliary "bond" variables $\{n_{ij}\}$,

$$\mathcal{P}[n|\sigma]=\prod_{i,j}\left[\frac{w_{ij}}{W_{ij}(\sigma_i,\sigma_j)}\delta_{n_{ij},0} +\left[1-\frac{w_{ij}}{W_{ij}(\sigma_i,\sigma_j)}\right]\delta_{n_{ij},1}\right]\ , \tag{B5}$$

such that given $\{\sigma\}$, the probability of laying down a bond between spins σ_i and σ_j (i.e., having $n_{ij}=1$) is zero if $W_{ij}(\sigma_i,\sigma_j)=w_{ij}$ (i.e., the spins σ_i and σ_j are aligned unfavorably) and $1-w_{ij}/W_{ij}(\sigma_i,\sigma_j)$ otherwise. From Eqs. (B3) and (B5), one can easily show that

$$\mathcal{P}[\sigma,n]=\prod_{i,j}\{w_{ij}\delta_{n_{ij},0}+[W_{ij}(\sigma_i,\sigma_j)-w_{ij}]\delta_{n_{ij},1}\} \tag{B6}$$

and

$$\mathcal{P}[\sigma|n]=\prod_{(i,j):n_{ij}=1}[W_{ij}(\sigma_i,\sigma_j)-w_{ij}]\ , \tag{B7}$$

where the product is taken over those pairs (ij) having $n_{ij}=1$, so that after tracing out the $\{n\}$ variables in Eq. (B7), Eq. (B3) for $\mathcal{P}[\sigma]$ remains valid. Equation (B7) shows that for any given bond configuration $\{n\}$, the only spin configurations with nonzero probability are those having bonded spins aligned favorably. Moreover, if a pair of spins σ_i and σ_j that are bonded with $n_{ij}=1$ are flipped together, the probability remains unchanged.

The prescribed embedded spins Swendsen-Wang method begins by first embedding the spin variables $\{\sigma\}$ into the continuous fields $\{s\}$ whose magnitudes are now frozen. Then the equilibration proceeds by alternately addressing $\{n\}$ and $\{\sigma\}$. First given the configuration $\{\sigma\}$, bonds $\{n\}$ are laid down between pairs of spins according to Eq. (B5). Then given the bond configuration $\{n\}$, each block of bonded spins can be flipped simultaneously with 50% probability without changing the probability Eq. (B7). Unconnected spin blocks are flipped independently from each other. After this the original continuous fields $\{s\}$ are restored, using the new spin variables. This completes one cycle of the Swendsen-Wang sweep.

*Permanent address: Department of Chemistry, University of Southern California, Los Angeles, CA 90089-0482.

[1] See, for example, J. Ulstrup, *Charge Transfer Processes in Condensed Media* (Springer, Berlin, 1979).
[2] J. Völkl and G. Alefeld, in *Hydrogen in Metals,* edited by G. Alefeld and J. Vökl (Springer, New York, 1978).
[3] See, for example, R. F. Voss and R. A. Webb, Phys. Rev. Lett. **47**, 265 (1981).
[4] See, for example, R. de Bruyn Ouboter, Physica B (Utrecht) **126**, 423 (1984).
[5] For a review, see A. J. Leggett, S. Chakravarty, A. T. Dorsey, M.P.A. Fischer, A. Garg, and W. Zwerger, Rev. Mod. Phys. **59**, 1 (1987).
[6] A. J. Bray and M. A. Moore, Phys. Rev. Lett. **49**, 1545 (1982).
[7] T. Holstein, Ann. Phys. (N.Y.) **8**, 343 (1959); Y. Toyazawa, in *Polarons and Excitons,* edited by C. G. Kuper and G. D. Whitefield (Plenum, New York, 1963), p. 211; H. B. Shore and L. M. Sanders, Phys. Rev. B **7**, 4537 (1973); R. Pirc and J. A. Krumhasal, *ibid.* **11**, 4470 (1975).
[8] S. Chakravarty and A. J. Leggett, Phys. Rev. Lett. **52**, 5 (1984).
[9] H. Grabert and U. Weiss, Phys. Rev. Lett. **54**, 1605 (1985); U. Weiss, H. Grabert, P. Hänggi, and P. Riseborough, Phys. Rev. B **35**, 9535 (1987).
[10] A. Garg, Phys. Rev. B **32**, 4746 (1985).
[11] R. A. Harris and L. Stodolsky, J. Chem. Phys. **74**, 2145 (1981); R. Silbey and R. A. Harris, *ibid.* **80**, 2615 (1984).
[12] E. C. Behrman, G. A. Jongeward, and P. G. Wolynes, J. Chem. Phys. **79**, 6277 (1983); E. C. Behrman and P. G. Wolynes, *ibid.* **83**, 5863 (1985).
[13] B. Carmeli and D. Chandler, J. Chem. Phys. **82**, 3400 (1985); **89**, 452 (1988).
[14] D. Chandler, in Liquids, Freezing, and the Glass Transition, Les Houches 51, Part 1, edited by D. Levesque, J. P. Hansen, and J. Zinn-Justin (Elsevier Science, North-Holland, 1991), p. 193.
[15] J. Kondo, Physica B **125**, 279 (1984); J. Kondo, in *Fermi Surface Effects,* Springer Series in Solid State Sciences Vol. 77 edited by J. Kondo and A. Yoshimori (Springer-Verlag, Berlin, 1988).
[16] K. Yamada, Prog. Theor. Phys. **72**, 195 (1984); K. Yamada, A. Sakurai, and S. Miyazima, *ibid.* **73**, 1342 (1985).
[17] L.-D. Chang and S. Chakravarty, Phys. Rev. B **31**, 154 (1985).
[18] M. Sassetti and U. Weiss, Phys. Rev. Lett. **65**, 2262 (1990).

[19] R. Kubo and Y. Toyazawa, Prog. Theor. Phys. **13**, 163 (1955); N. R. Kestner, J. Logan, and J. Jortner, J. Phys. Chem. **78**, 2148 (1974).
[20] A. O. Caldeira and A. J. Leggett, Phys. Rev. Lett. **46**, 211 (1981); Ann. Phys. (N.Y.) **149**, 374 (1983).
[21] W. Zwerger, Z. Phys. B **53**, 53 (1983); **54**, 87 (1983).
[22] C. H. Mak and D. Chandler, Phys. Rev. A **41**, 5709 (1990).
[23] V. S. Filinov, Nucl. Phys. B **271**, 717 (1986).
[24] J. D. Doll and D. L. Freeman, Adv. Chem. Phys. **73**, 289 (1988); J. D. Doll, D. L. Freeman, and M. J. Gillan, Chem. Phys. Lett. **143**, 277 (1988); J. D. Doll, T. L. Beck, and D. L. Freeman, J. Chem. Phys. **89**, 5753 (1988).
[25] N. Makri and W. H. Miller, Chem. Phys. Lett. **139**, 10 (1987); N. Makri and W. H. Miller, J. Chem. Phys. **89**, 2170 (1988).
[26] J. D. Doll, R. D. Coalson, and D. L. Freeman, J. Chem. Phys. **87**, 1641 (1987); J. Chang and W. H. Miller, *ibid.* **87**, 1648 (1987).
[27] R. E. Cline, Jr. and P. G. Wolynes, J. Chem. Phys. **88**, 4334 (1988).
[28] D. Chandler and P. G. Wolynes, J. Chem. Phys. **74**, 4078 (1981).
[29] J. Hubbard, Phys. Rev. Lett. **3**, 77 (1959); R. L. Stratonovich, Dokl. Akad. Nauk SSSR **115**, 1097 (1958) [Sov. Phys.—Dokl. **2**, 416 (1958)].
[30] L. S. Shulman, *Techniques and Applications of Path Integration* (Wiley, New York, 1981), Chap. 19.
[31] W. H. Miller, Adv. Chem. Phys. **25**, 69 (1974); **30**, 77 (1975).
[32] S. Coleman, in *The Whys of Subnuclear Physics,* edited by A. Zichichi (Plenum, New York, 1979).
[33] T. L. Beck, J. D. Doll, and D. L. Freeman, J. Chem. Phys. **90**, 3181 (1989).
[34] N. Metropolis, A. W. Rosenbluth, M. N. Rosenbluth, A. H. Teller, and E. Teller, J. Chem. Phys. **21**, 1087 (1953).
[35] R. C. Brower and P. Tamayo, Phys. Rev. Lett. **62**, 1087 (1989).
[36] R. H. Swendsen and J.-S. Wang, Phys. Rev. Lett. **58**, 86 (1987).
[37] See also, U. Wolff, Phys. Rev. Lett. **60**, 1461 (1988); D. Kandel, E. Domany, D. Ron, A. Brandt, and E. Loh, Jr., *ibid.* **60**, 1591 (1988); F. Niedermayer, *ibid.* **61**, 2026 (1988).
[38] R. G. Edwards and A. D. Sokal, Phys. Rev. D **38**, 2009 (1988).
[39] Numerator and denominator are accumulated simultaneously according to Eq. (6.8). They both suffer from the sign problem.
[40] D. Chandler, *Introduction to Modern Statistical Mechanics* (Oxford, New York, 1987), Chap. 5.
[41] M. Sassetti and U. Weiss, Phys. Rev. A **41**, 5383 (1990).
[42] See, for example, M. J. Gillan, J. Phys. C **20**, 3621 (1987), and references therein.